Discrete Femtolitre Pipetting with 3D Printed Axisymmetrical Phaseguides

Blankespoor, Maarten; Manzaneque, Tomás; Ghatkesar, Murali Krishna

Important note
To cite this publication, please use the final published version (if applicable).
Please check the document version above.

Discrete Femtolitre Pipetting with 3D Printed Axisymmetrical Phaseguides

Maarten Blankespoor, Tomás Manzaneque, and Murali Krishna Ghatkesar*

The capacity to precisely pipette femtoliter volumes of liquid enables many applications, for example, to functionalize a nanoscale surface and manipulate fluids inside a single-cell. A pressure-controlled pipetting method is the most preferred, since it enables the widest range of working liquids. However, precisely controlling femtoliter volumes by pressure is challenging. In this work, a new concept is proposed that makes use of axisymmetrical phaseguides inside a microfluidic channel to pipette liquid in discrete steps of known volume. An analytical model for the design of the femtopipettes is developed and verified experimentally. Femtopipettes are fabricated using a multi-scale 3D printing strategy integrating a digital light processing printed part and a two-photon-polymerization printed part. Three different variants are designed and fabricated with pipetting resolutions of 10 picoliters, 180 femtoliters and 50 femtoliters. As a demonstration, controlled amounts of a water-glycerol mixture were first aspirated and then dispensed into a mineral oil droplet.

1. Introduction

Understanding the internal processes of cells is of paramount importance for biology and medicine. Assessing the properties of individual cells is a topic of increasing scientific efforts. Classical methods usually involve steps to sort and/or isolate the cells of interest, after which the cells are opened by lysis or microdissection to gain access to the cell content.[1,2] Although a lot of insight can be gained this way, obvious disadvantages of such methods are that cells are analyzed away from their natural environment and are often killed in the process. New and innovative physical

M. Blankespoor, M. K. Ghatkesar
Department of Precision and Microsystems Engineering
Delft University of Technology
Mekelweg 2, Delft 2628CD, The Netherlands
E-mail: m.k.ghatkesar@tudelft.nl
T. Manzaneque
Department of Microelectronics
Delft University of Technology
Mekelweg 4, Delft 2628CD, The Netherlands

The ORCID identification number(s) for the author(s) of this article can be found under https://doi.org/10.1002/smtd.202300942

and biochemical methods have been proposed more recently, that study the contents of cells while they stay alive.[3] These methods are based on the controlled transport of substances of interest through the cell membrane and several principles have been investigated for this purpose.[4] Among these principles, the physical method of penetrating a chosen single cell by a micro or nano-scaled pipette is a very promising and versatile technique due to its positional accuracy and the possibility for both extraction and delivery of substances.[5]

Miniaturized pipettes with working volumes in the range of femtoliters, hereafter femtopipettes, have been classically fabricated by heating and pulling a glass tube, achieving nanometer-sized apertures.[6,7] The use of such femtopipettes in experiments with cells requires accurate positioning that often relies on visual feedback, and it is difficult to assess whether the targeted cell is indeed penetrated or not.[8] An extension to the functionality of the femtopipette was made when a cantilever for an atomic force microscope (AFM) was made out of a microfluidic channel.[9] The microfluidic AFM cantilever was connected to a pressure source such that liquid could be forced through an aperture at the tip. The technique was called fluid force microscopy or 'FluidFM'.[10] The force feedback provided by the AFM system proved useful to detect contact with the cell and even the penetration of the cell membrane. With this method, successful injection and aspiration of cell contents have been demonstrated on living cells.[11–15] Furthermore, cell adhesion strength measurements and pick-and-place functionality have been demonstrated using the FluidFM method.[16,17]

Despite these successes, a major challenge remains in the fabrication of cantilevers with microfluidic channels embedded. Most of the current implementations involve complex processes based on multiple steps of 2D lithography and standard microfabrication technologies, hindering design freedom.[18] An advancement in fabrication was provided by Kramer et al., when they made a fully functional microfluidic AFM cantilever by means of a multi-scale 3D printing method.[19] Using a hybrid 3D printing fabrication process that combines digital light processing with two-photon-polymerization (2PP) allowed for improving design freedom and prototyping speed from weeks to days.

For controlled transport of substances into the cell through the cell membrane within a liquid environment, three different
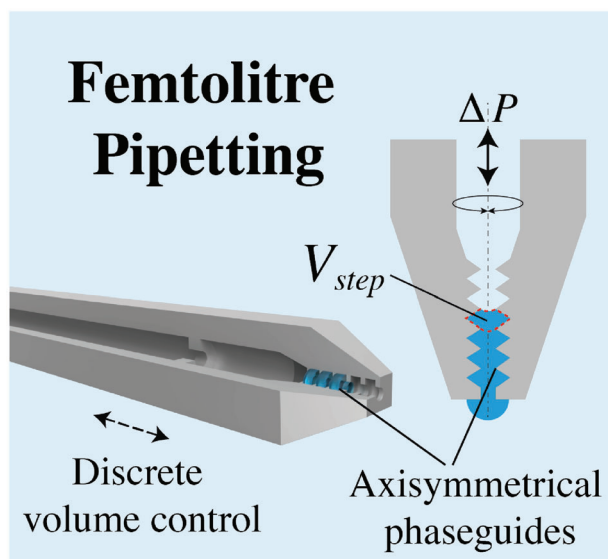
Figure 1. Schematic representation of the proposed pipette, using axisymmetrical phaseguides to control discrete, femtoliter volumes.

principles have been reported: thermal, electrochemical, and pressure-based. The first two have been able to obtain volume resolutions down to the attoliter level (1 aL = 10^{-18} L).[20,21] Nevertheless, these techniques need working liquids with special properties (like metallic nanoparticles or conducting fluid), which limits their suitability for experiments of relevance in cell biology. Pressure remains the most straightforward principle to use, allowing for the widest range of substances to be handled. However, the volume resolution of pressure-based methods is relatively low, with the best results in literature coming down to approximately 100 femtoliters (1 fL = 10^{-15} L) of dispensed or aspirated liquid, albeit with limited precision.[11,12,22]

This research is aimed to increase the volume dosing resolution and precision of pressure-driven femtopipetting systems. For this purpose, a new femtopipette concept is proposed based on the multi-scale 3D printing methods reported before.[19,23] The concept makes use of capillary pinning locations, also known as 'phaseguides'[24] or 'capillary valves',[25] where the meniscus formed at the liquid-air interface pins predictably to designated locations (**Figure 1**). This phenomenon is used to provide discrete steps of known volume, adjustable by the device design and without relying on the accuracy of the applied pressure.

2. Theory

At the liquid-gas interface in capillary tubes, liquid forms a meniscus due to the surface tension of the liquid and the contact angle between the liquid and the tube walls. Laplace pressure $\Delta P_{Laplace}$ (2) acts on this meniscus, giving rise to capillarity. The liquid advancement due to capillarity can be perturbed by changing the internal diameter of the channel. Here, we analyze this effect. The pressure balance of a liquid inside a straight-walled channel (see **Figure 2**A) is given by

$$\Delta P_{total} = \Delta P_{Laplace} - \Delta P_{applied} \tag{1}$$

Here, all pressures are relative to the atmospheric pressure, and ΔP_{total} signifies the pressure difference between both sides of the liquid-air meniscus. The applied pressure $\Delta P_{applied}$ is defined positive for gas pressure greater than the pressure in the liquid. The sign of the pressure ΔP_{total} determines whether the liquid will enter the channel (positive) or be expelled from the channel (negative). Under the absence of applied pressure ($\Delta P_{applied} = 0$), the capillary behavior is determined only by the Laplace pressure $\Delta P_{Laplace}$ which is given as

$$\Delta P_{Laplace} = \frac{2\gamma}{R} = \frac{4\gamma \cos(\theta)}{d} \tag{2}$$

where γ is the surface tension of the interface, R is the radius of curvature of the meniscus, d is the diameter of the channel and θ is the contact angle. Note that $\Delta P_{Laplace}$ is positive for $\theta < 90°$ (hydrophilic) and negative for $\theta > 90°$ (hydrophobic). Note that this model is only valid for micro-capillaries where effects of gravity can be neglected.

2.1. Liquid Advancement

Here, we describe the situation where the liquid advancement inside a hydrophilic channel due to capillarity can be perturbed by changing the internal diameter of the channel. We introduce an angle α that describes half the meniscus arc and is by definition complementary to the contact angle θ, see Figure 2A. Thus, when the meniscus remains within a straight-walled channel with constant diameter d, it follows that $\alpha = 90° - \theta$.

If the meniscus reaches a point where the channel expands axisymmetrically with a certain expansion angle β, the edges of the meniscus will pivot around the corner edge to re-establish the contact angle between the liquid and the slanted walls (Figure 2B,C). The radius of curvature R therefore increases, and the Laplace pressure will decrease according to Equation (2). In this situation, $\alpha = 90° - \theta - \beta$. To include such geometrical changes of the channel, Equation (2) can be re-written as

$$\Delta P_{Laplace} = \frac{4\gamma \sin(\alpha)}{d} \tag{3}$$

The liquid will be able to advance beyond the axisymmetrical expansion for β below a critical value $\beta_{c1} = 90° - \theta$. For β equal to or greater than the critical angle β_{c1} (Figure 2D), the advancement of the meniscus beyond the expansion causes α to become respectively zero or negative. At exactly $\beta = \beta_{c1}$, $\alpha = 0°$ and $R = \infty$ (flat meniscus, indicated with red line in Figure 2D). Therefore, the Laplace pressure reduces to zero, effectively stopping the capillary advancement. In cases where $\beta > \beta_{c1}$, the hypothetical advancement of the meniscus beyond the expansion would change the interface shape from concave to convex ($\alpha < 0°$). Therefore, a negative Laplace pressure would force the meniscus to settle in an equilibrium position that corresponds to a flat shape ($\alpha = 0°$). In other words, for channel expansions with $\beta \geq \beta_{c1}$ the liquid meniscus pins to the corner of the expansion in the absence of applied pressure. Such a geometry is called a phaseguide.[26]
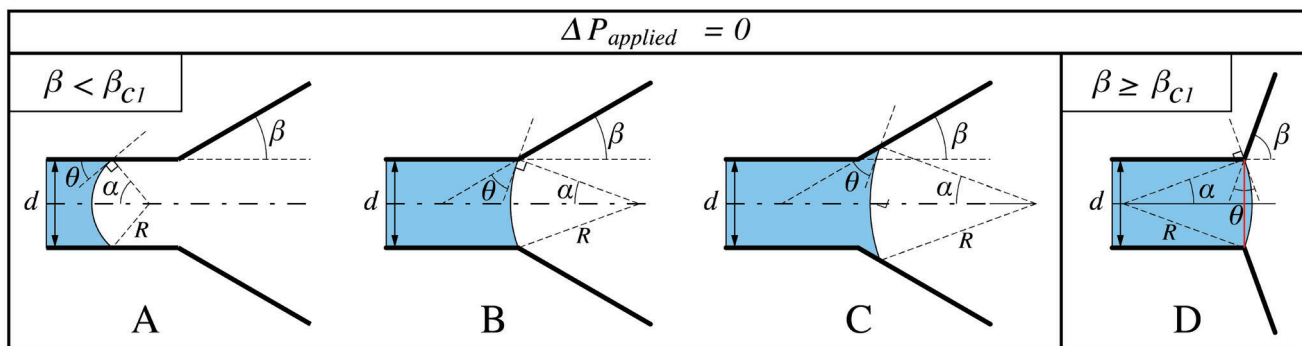
Figure 2. Advance of liquid inside a hydrophilic channel due to capillarity. A) Meniscus in straight-walled channel with constant diameter d, where $\alpha = 90° - \theta$. B) Meniscus reaching an axisymmetrical channel expansion of angle β, where the contact angle is fulfilled at the slanted walls such that $\alpha = 90° - \theta - \beta$. C) For $\beta < \beta_{c1}$, the meniscus will advance beyond the channel expansion, with a progressive decrease of the Laplace pressure due to increasing meniscus radius R. D) For $\beta \geq \beta_{c1}$, the meniscus stops, $\alpha = 0°$ (shown as a line in red), the Laplace pressure reduces to zero and the liquid advancement is stopped, effectively pinning the meniscus to the expansion edge.

2.2. Gas Advancement

Here, we analyze the scenario in which gas is forced into a hydrophilic capillary previously filled with liquid, by applying positive gas pressure slightly greater than the Laplace pressure ($\Delta P_{applied} > \Delta P_{Laplace}$, see **Figure 3**). When the meniscus is inside the straight-walled part with constant diameter d (Figure 3A), the pressure balance is once again given by Equations (1) and (3), with $\alpha = 90° - \theta$. This relation still holds when the meniscus pins at the channel expansion and is held there by applying a pressure equal to the Laplace pressure (Figure 3B). Increasing the applied pressure at this point will force the meniscus to pivot around the corner to re-establish the contact angle θ with the slanted walls. In this case α is re-defined as $\alpha = 90° - \theta + \beta$ (see Figure 3C). Substituting this in Equation (3) gives the maximum applied pressure ($\Delta P_{applied}$) for which the meniscus in a phaseguide with a certain expansion angle β will remain pinned. The maximum Laplace pressure occurs when the meniscus' radius of curvature R is minimal, i.e., for $R = d/2$, with $\alpha = 90°$. This condition defines a new 'critical angle' β_{c2} that equals the contact angle θ in this scenario.

If the expansion angle is greater than the critical angle, $\beta \geq \beta_{c2}$, (see Figure 3D) and the applied pressure is increased beyond the Laplace pressure, the meniscus will progress through its minimal radius (i.e., maximal Laplace pressure, indicated with green) before it can establish the contact angle θ on the slanted walls. The larger radius R of the meniscus that is necessary to establish the contact angle θ on the slanted walls (indicated with red) would cause the opposing Laplace pressure to decrease, resulting in the gas 'bursting' into the subsequent channel section. The applied gas pressure needed to force the meniscus through a channel expansion is called burst pressure (relative to the atmospheric pressure), and can be expressed as:

$$\Delta P_{burst} = \begin{cases} \dfrac{4\gamma \sin(\alpha)}{d} & \text{for } \alpha < 90°, \beta < \beta_{c2} \\[2ex] \dfrac{4\gamma}{d} & \text{for } \alpha \geq 90°, \beta \geq \beta_{c2} \end{cases} \qquad (4)$$

If $\Delta P_{applied} > \Delta P_{burst}$, the sign of ΔP_{total} in Equation (1) becomes negative, indicating that the liquid meniscus is being expelled
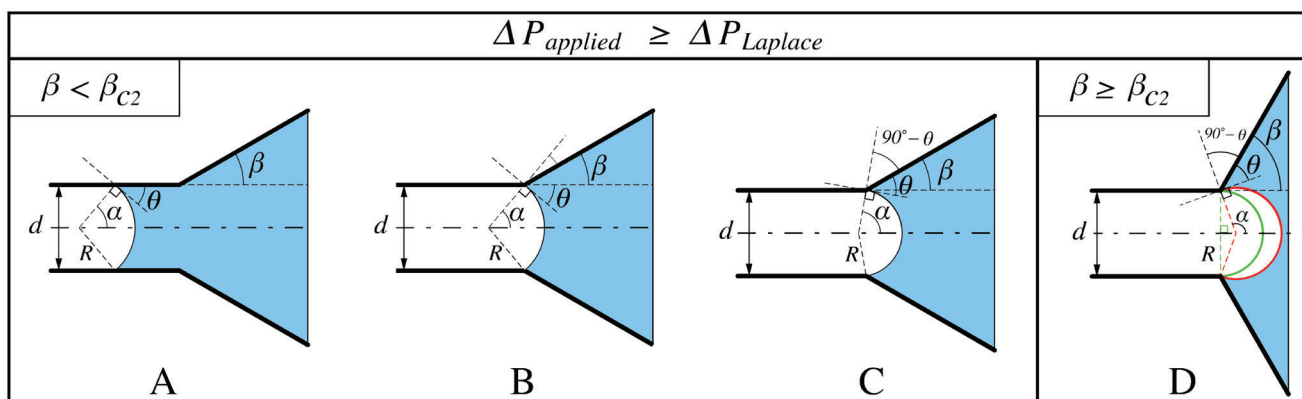
Figure 3. Forced retreating liquid meniscus due to increased applied gas pressure $\Delta P_{applied}$ (applied from the left). A) Situation comparable to Figure 2A, where the meniscus is in straight-walled capillary and $\alpha = 90° - \theta$. B) α remains the same as in (1) unless $\Delta P_{applied}$ is increased. C) When $\Delta P_{applied}$ is increased, the meniscus changes its curvature and α is defined as $\alpha = 90° - \theta + \beta$. D) For angles $\beta \geq \beta_{c2}$, the meniscus will progress through its minimal radius R causing the burst pressure to reach its maximum, $\Delta P_{burst} = \frac{4\gamma}{d}$.

**ADVANCED
SCIENCE NEWS**

www.advancedsciencenews.com

**small
methods**

www.small-methods.com

Figure 4. Overview of the complete device. A) Device setup with the fluid interface (1) installed on holder (4) for experimenting and connected to a pressure source with a flexible tubing (Tygon ND-100-80 Microbore, ID 1.02mm, OD 1.78mm) (3). B) Schematic cross-sectional view of the fluid interface showing the internal channel (1) connecting to the laser-drilled aperture (2) which leads to the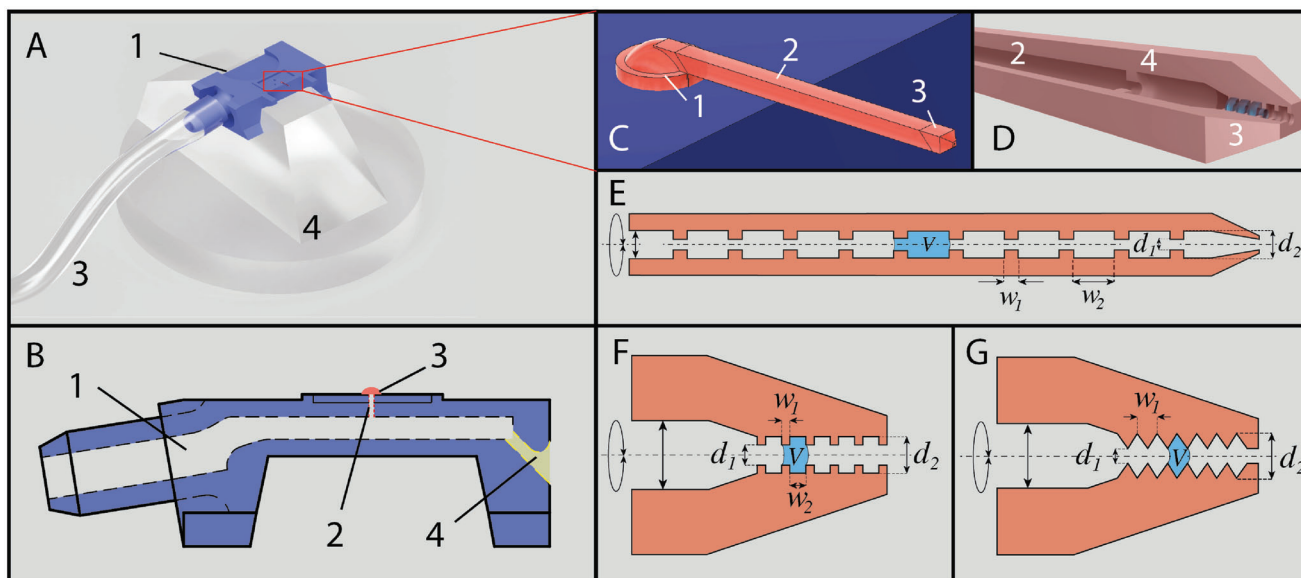 2PP printing site (3). The purge channel (4) facilitates development during fabrication and can be plugged later. C) Enlargement of CAD image of the femtopipette consisting of three parts: the dome (1), sealing the aperture; the hollow cantilever (2) which is suspended horizontally to protrude over the edge of the fluid interface; and the nozzle (3) in which stepped, axisymmetrical phaseguides are embedded. D) Cut out section of cantilever CAD model with exposed internal channel (2) connecting to the pressure source; a nozzle (3) with stepped, axisymmetrical phaseguides of which three are shown 'filled' and a large 'backup' phaseguide (4) to better control aspiration volume. E–G) Schematic representations of three axisymmetrical phaseguide geometries with definition of used dimensions (see Table 1).

from the channel. In literature, the burst pressure is also referred to as 'bubble point pressure' for $\alpha \geqslant 90°$.[27] Equation (4) predicts that the burst pressure will plateau for expansion angles above the critical value β_{c2}.

3. Design

A fabrication process based on multi-scale 3D printing was used to demonstrate the proposed concept.[19,23] The femtopipette device consists of a combination of two parts, 3D printed by different methods. The micro-scaled part of the device is 3D printed using two-photon-polymerization (2PP). This part is printed on top of a 'fluid-interface' part that serves as mechanical support and provides fluidic connections. This fluid-interface is 3D printed at the millimeter scale using a digital light processing (DLP) stereolithography printer.

3.1. Fluid Interface

The fluid interface allows the femtopipette to be easily handled and connected to a pressure source. An overview of the fluid interface holder is shown in **Figure 4**A.

In order to reduce the printing time of the femtopipette with 2PP, an aperture of minimal size is needed to connect the internal channels of the fluid interface (Figure 4B) to the femtopipette. The capability of the used DLP printer to print small apertures in the order of $\approx 100\mu m$ was insufficient. Therefore, the interfaces

were first DLP-printed without aperture, and the top surface aperture was drilled with a high-resolution laser cutter (Figure 4B,2). Arrays of fluid interfaces were printed on sacrificial supports inside a specially designed support-cup that fits the sample holder (25mm X 25mm) of the used 2PP printer. Refer to the, Section S1 (Supporting Information), for more details on the design of the fluid interface.

3.2. Femtopipette

The femtopipette was designed as a suspended hollow cantilever that protrudes over the edge of the fluid interface (as illustrated in Figure 4C). With this configuration, the suspended hollow cantilever is shown to be capable of acting as a probe with AFM functionality.[19,23] Distinguishing between different parts (dome (1), cantilever (2), and nozzle (3)) permits to set specific 2PP printing parameters separately, which facilitates print optimization (see Section 6.1.2, specifically Table 2). A 'back-up' phaseguide (Figure 4 (D, 4)) was implemented such that it would be easier to contain the fluid when manually filling the nozzle. The dome was designed such that it could be printed within the writing field of the 2PP printer (200µm diameter) without block stitching—an improvement over our previous work.[23]

Different variants and sizes of axisymmetrical phaseguides were designed and tested (see Figures 4E–G). The design freedom gained by employing the 2PP printing technique enables to adjust the desired dosing volume by reshaping the phaseguide geometry. The volume of one dosing step is determined by

**ADVANCED
SCIENCE NEWS**

www.advancedsciencenews.com

**small
methods**

www.small-methods.com

Table 1. Dimensions of three different variants of axisymmetrical phaseguides, as defined in Figure 4E-G. All values for d_1, d_2, w_1, w_2 are in microns (µm). Shrinkage values are calculated with respect to the designed volume.

	Design						SEM measurement						Shrinkage %
	d_1	d_2	w_1	w_2	V_{step}	V_{total}	d_1	d_2	w_1	w_2	V_{step}	V_{total}	
Rectangular picolitre phaseguides (Figure 4E)	8	20	10	30.23	10 pL	100 pL	8.27	19.81	9.00	30.52	9.89 pL	98.9 pL	1.10%
Rectangular femtolitre phaseguides (Figure 4F)	4	8	7.958	1.989	200 fL	2 pL	4.20	7.86	6.32	1.93	181.1 fL	1.81 pL	9.45%
Triangular femtolitre phaseguides (Figure 4G)	3.6	7	2.63	—	60 fL	600 fL	3.73	6.77	2.41	—	53.6 fL	535.6 fL	10.73%

the void-volume between two successive channel expansions (phaseguides). These expansions can take different forms as long as the expansion angle β remains larger than the critical angle β_{c1} (as defined in Section 2.1). In this research, two such geometrical variants are treated: 1) rectangular axial revolutions (Figure 4E,F) where the void-volume per step is given as

$$V_{step} = \frac{1}{4}\pi(d_1^2 w_1 + d_2^2 w_2) \tag{5}$$

and 2) triangular axial revolutions (Figure 4G) where the void-volume is

$$V_{step} = \frac{1}{12}\pi w_1(d_1^2 + d_1 d_2 + d_2^2) \tag{6}$$

with parameters d_1, d_2, w_1, and w_2 as defined in Figure 4E–G. The dimensions used are tabulated in **Table 1**. More details on the

design of the femtopipette can be found in the Section S2 (Supporting Information).

4. Results & Discussion

4.1. Fabrication

The DLP printing of the fluid interfaces took 80 min and the resulting channels were rarely clogged nor difficult to clean using the standard cleaning protocol (See Section S1, Supporting Information). Images of the resulting devices are shown in **Figure 5** with incremental enlargements. A printed cross section of the entire femtopipette is shown in Figure 5D. Upon inspection with the optical microscope, the diameter of the laser drilled apertures was measured, giving 60µm ± 10µm. Sometimes small cracks could be seen around the aperture, likely due to heat stress during lasering. Overall, the apertures looked clean (see inset Figure 5 B1): without the rounded edges due to DLP printing experienced
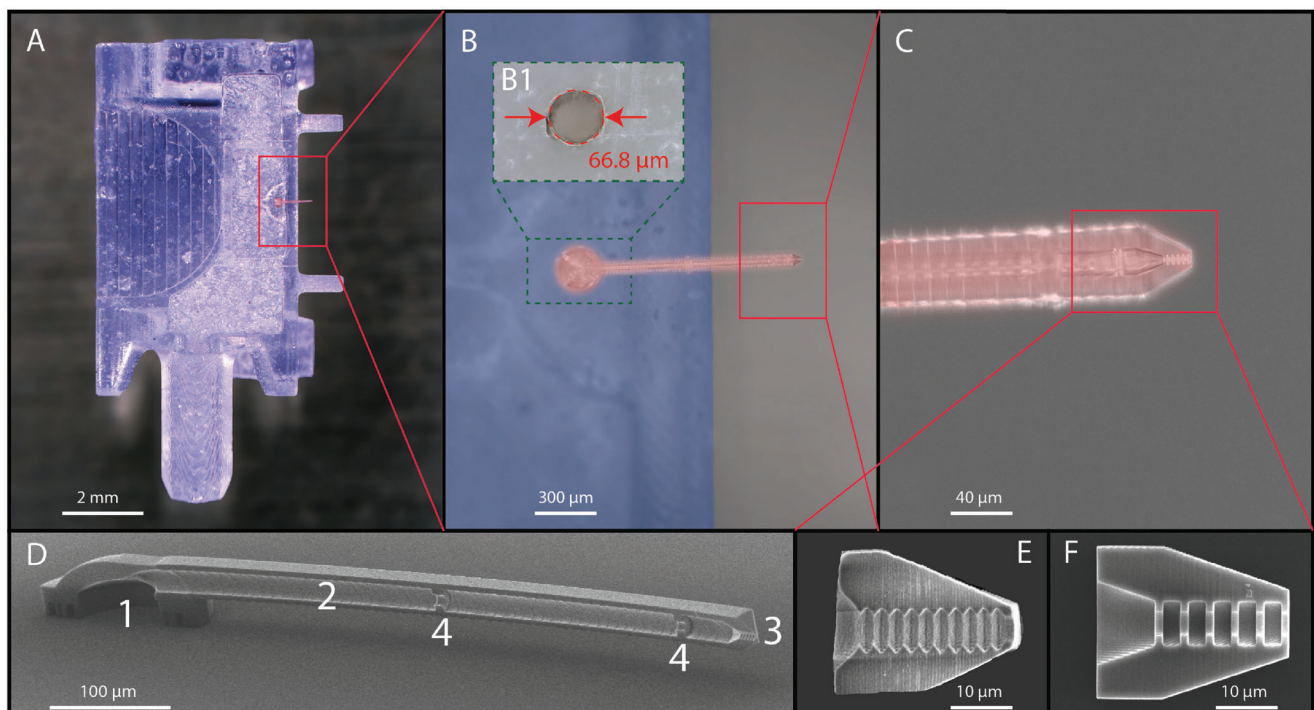
Figure 5. Resulting device overview. A–C) Optical micrographs of the fluid interface (blue tint) with femtopipette (red tint) on top. Inset B1) Optical micrograph of laser-drilled aperture (not to scale, true color) before 2PP printing. D) SEM image of 2PP printed open cross-section of the femtopipette with dome (1), channel (2), nozzle (3) and large 'backup' phaseguides (4). E,F) SEM images of 2PP printed cross-sections exposing two nozzle designs. SEM measurements of the dimensions are listed in Table 1.

**ADVANCED
SCIENCE NEWS**

www.advancedsciencenews.com

**small
methods**

www.small-methods.com

Figure 6. Contact angle and burst pressure measurement. A) Schematic of cantilever with 12 successive expansions (phaseguides) with increasing expansion an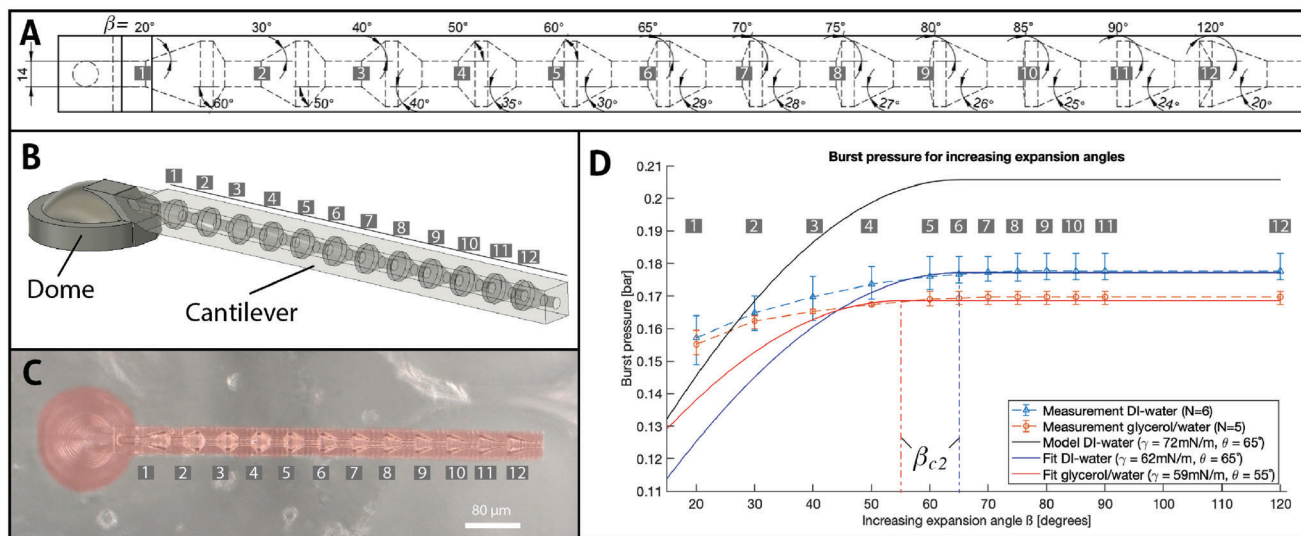gle β (left to right) as defined in Figures 2 and 3. B) CAD model showing 3D representation of axisymmetrical expansions. C) Optical micrograph showing 2PP printed device (red tint) on top of fluid interface. D) Plot of burst pressure measured at each step, compared to the analytical model prescribed by Equation (4).

in our previous work.[23] Due to the small aperture size, the dome part of the femtopipette needed no block stitching and was 2PP printed in one writing field in 7 min (compared to ≈60 minutes in our previous work[19,23]). The cantilevers were 600μm long and were printed in 18 min. The nozzle was printed in ≈5–8 min, depending on the chosen phaseguide geometry.

The 2PP printing started 5μm below the found interface, which ensured a secure, leak-free attachment of the dome in most cases, tested to withstand at least 4.5 bar. When the 2PP laser reached the surface, tiny bubbles could be observed through the process-camera feed, confirming contact with the interface. To prevent unwanted polymerization of the void channel regions, the dose was lowered when printing the nozzle section. The lower dose did result in higher shrinkage during development, reducing the void volume up to 10.73% with respect to the designed void volume, depending on the dose (see Table 1). To find the limit of this fabrication technique, smaller step volumes (down to 10 fL) were also attempted, but these failed due to the unsuccessful removal of the unpolymerized resin inside the channel during the development step resulting in clogging.

4.2. Device Characterization

For the purpose of validating the proposed analytical model (Equation (4)), a dedicated device was designed and fabricated with successive axisymmetrical expansions having increasing expansion angles β, schematically shown in **Figure 6**A. The expansion angles β were varied for both inward and outward direction. This device thus serves two purposes: 1) to assess the static contact angle between the cantilever and the fluid inside its channel, and 2) to measure the burst pressure of the meniscus in relation to the expansion angle β.

4.2.1. Contact Angle Measurement

From literature, the static contact angle between water and cured IP-Dip was suggested to be in the range from 72°[28] to 80.5°.[29] As an extra reference, a macro-scale contact angle measurement was performed on spincoated IP-Dip with an optical tensiometer (see Section 6.2.1 for details) resulting in a macro-scale contact angle θ of 62.3° ± 4.8° (N=18).

To ascertain that this contact angle also holds for microscale structures, the aforementioned device (Figure 6B,C) was used. The liquid entered the cantilever spontaneously by means of capillary action, until the critical angle β_{c1} was met—depending on the contact angle θ of the liquid with the cantilever walls (as described in Section 2.1). The point where the liquid stopped thus gave an indication of the static contact angle according to $\theta = 90° - \beta_{c1}$. Pinning was observed at expansion angles β from 24° to 30° (for N=5 different cantilevers) yielding an approximate static contact angle θ between 66° and 60°, respectively. This is in good agreement with the measurement conducted with the optical tensiometer.

4.2.2. Burst Pressure Measurement

After observing the static contact angle in absence of applied pressure, the cantilever was emptied and was filled by applying negative pressure inside the cantilever. When the cantilever was filled, the pressure was equalized. Then, the applied gas pressure was slowly increased inside the cantilever, allowing the device and pressure measurement system to reach steady state. While pushing the liquid-air meniscus outwards (Figure 3), the burst pressure ΔP_{burst} as a function of the expansion angle β was recorded for each expanding step. The meniscus was observed to pin to each phaseguide, as expected. Then, when the applied air

**ADVANCED
SCIENCE NEWS**

www.advancedsciencenews.com

**small
methods**

www.small-methods.com

pressure was sufficient, i.e. $\Delta P_{applied} > \Delta P_{burst}$, the meniscus would burst through, and pin to the next phaseguide with increased expansion angle β (Video S5-1, Supporting Information).

The burst pressures were recorded and are shown in Figure 6D. In this figure, the analytical model prescribed by Equation (4) is plotted and compared to the measured burst pressures of DI-water (blue) and a 50% water-glycerol mixture (orange). As predicted by the model, a plateau in the burst pressure can be observed for expansion angles β greater than the critical angle β_{c2}. Note that in this scenario (gas advancement) the contact angle θ is equal to the critical angle β_{c2} (see Section 2.2). The level of the plateau is determined by the ratio of the surface tension γ over the channel diameter d, of which the latter is fixed at 14 µm—as designed and confirmed by optical measurement. The reference model (black) is plotted for the surface tension γ of DI-water at 72 mNm^{-1}, with the contact angle θ taken as 65° (as found in the previous section). The measurement data is fitted with the model by setting the surface tension γ and contact angle θ as fitting parameters. It becomes clear that the plateauing level of the measured DI-water data is lower than the reference, but the critical angle β_{c2} is in good agreement. The experiment was repeated with a water-glycerol mixture to strengthen the observation of the plateauing behavior. A slightly lower plateau is observed, together with a lower critical angle. This is expected because the surface tension as well as the contact angle of a water-glycerol mixture is known to be lower than that of pure water.[30]

It is difficult to say with certainty why the resulting burst pressures are lower than expected, but it could be argued that in practice, the surface tension of the liquid inside the channel is lowered due to contaminants left over from the chemical development process that act as surfactants. Another explanation could be that the air adjacent to the meniscus has a higher relative humidity, which could effectively lower the surface tension.[31] Furthermore, the deviation in the slope before the critical angle is not captured by our model and therefore it could be explained by the assumptions made. In particular, the model assumes sharp corners in the channel expansions, that in reality might be rounded at scales below the printing resolution (< 1 µm).

4.3. Controlled Dosing: Picolitre to Femtolitre Volumes

The liquid pinning behavior proved predictable and controllable, so as a step in the direction of functionality, the liquid dosing capabilities of axisymmetrical phaseguides were investigated. Several concepts were designed and tested (see Figure 4) with the goal of minimizing the dosing volume beyond the state-of-the-art of 100 fL. The feasibility of each concept was first confirmed while observing the liquid pinning when the femtopipette was submerged in DI-water and actuated with a manually operated syringe. An experiment was devised where one liquid was dosed inside another immiscible liquid. Two separate droplets were pipetted on a glass microscope slide: 1) 50:50 wt.% DI-water:Glycerol and 2) filtered mineral oil. First, the water-glycerol droplet was approached and entered with the femtopipette upon which negative pressure was applied with the syringe to aspirate a controlled amount of liquid. Then, the femtopipette was brought to the mineral oil droplet, where the water-glycerol mixture was dispensed in discrete steps, according to the volume contained within each

step between two successive axisymmetrical phaseguides. The diameter of the resulting droplet was measured to determine its volume (Video S5-2,3, Supporting Information).

Droplets that were dispensed into the mineral oil could be observed with the optical microscope due to the difference in refractive index. Images of the resulting droplets are shown in **Figure 7**A–C.

The volume was then calculated based on the assumption that the droplet formed a perfect sphere (in the case of the 10pL designed steps, Figure 7A) or a perfect half sphere (in the cases of the 200 and 60fL designed steps where the droplet was still partly adhered to the surface of the femtopipette, Figure 7B,C). Due to the hydrophilic properties of the cured IP-Dip, the droplet remained adhered to the femtopipette. Attempts to separate the droplet using ultrasound vibrations (sweep up to 1 MHz) were unsatisfactory. In further research, separation could potentially be realized with (local) chemical surface functionalization.

The measured average incremental volume steps V_{step} are 10.72 pL ± 7.9%, 180.0 fL ± 5.5% and 49.4 fL ± 8.9% for the three designs analyzed. These values are in good agreement with the void-volumes determined by SEM measurement (referring to Table 1).

It was also observed that when exiting the water-glycerol droplet, a small amount of liquid adhered to the outside of the femtopipette. This amount then beaded up when entering the oil, so that a small initial droplet was observed at the nozzle before the first step was taken. This explains the small initial volume offset which is especially visible in the 200 and 60fL designed steps (Figure 7B–E).

These demonstrations prove the concept of axisymmetrical phaseguides as a way to discretely dose liquid with unprecedented resolution. In principle, the achievable volume dosing resolution is only limited by the fabrication method, as it has been shown that the Laplace equations are still valid on a molecular scale.[32] Axisymmetrical phaseguides should also show meniscus pinning behavior when the system is hydrophobic,[33] which extends the range of possible working liquids and device materials. It is worth noting that the dosed volume does not depend on the properties of the liquid. Particularly, the shape of the meniscus depends on the surface tension and in turn on the liquid. Nevertheless, that holds on both the exit and entry points of the phaseguide, so that the net volume stays independent of the surface tension.

5. Conclusion

In this work, a new type of femtopipette has been developed that is able to control discrete amounts of liquid. To the best of the authors' knowledge, the demonstrated dosing resolution of 49.4 fL ± 8.9% is the best that pressure-actuated in-liquid dosing has reached. The use of axisymmetrical phaseguides enables controllable and repeatable in-liquid dosing that is straightforward to use without requiring a fine control of the applied pressure and even allows a manually operated syringe as pressure source.

The application of multi-scale 3D printing has proven valuable for concept iterations, design freedom, and production time. A functional device can be fabricated and tested over the course of two days. The introduction of a laser-drilled aperture in the
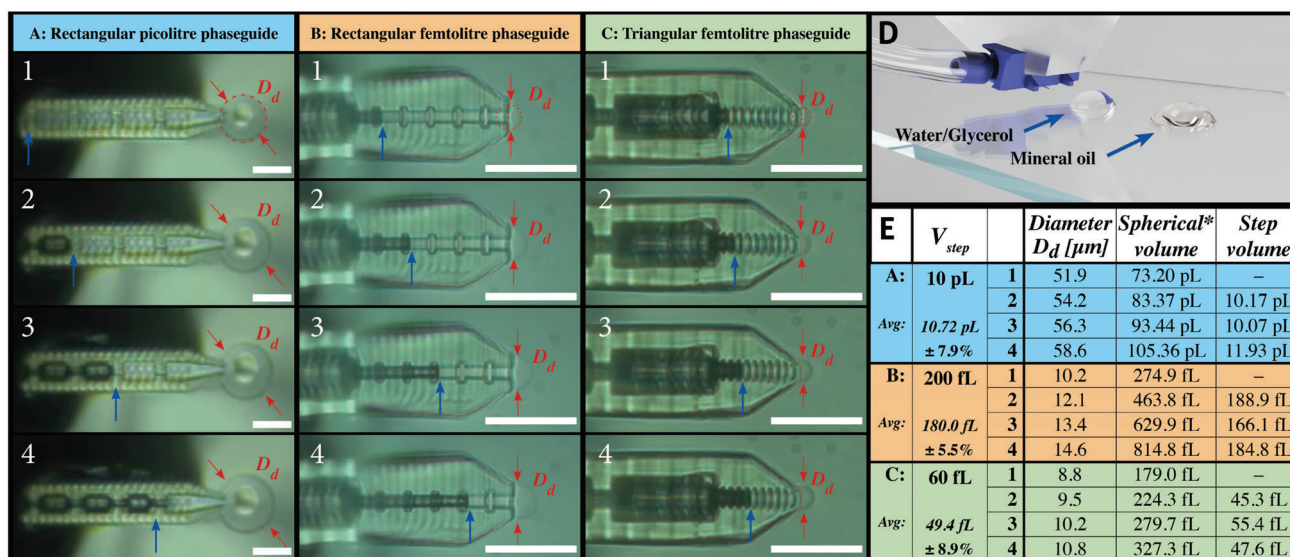
Figure 7. Discrete dispensing of water-glycerol droplet into mineral oil. A–C) Images are taken with an inverted microscope below the sample. The meniscus is indicated with a blue arrow. The droplets are created by applying pressure with a manually operated syringe connected to the femtopipette. The diameter of the droplets is denoted as D_d. The scale bar (white) is 40µm in all figures. Four incremental steps are shown (Note that for (A) only the last 4 steps out of 10 are shown). D) Impression of the experiment. The femtopipette is installed on an AFM motion stage and first approaches the water-glycerol droplet to aspirate a small amount, which is then dispensed into the mineral-oil droplet. E) Tabulated results, displaying both designed V_{step} and measured average V_{step} in italics. *Droplets were assumed spherical (A) or half spherical (B,C).

fluid interface significantly reduced 2PP printing time compared to previous works.

The existing analytical model for capillary pressure has been extended for predicting the geometry-dependent burst pressure when compelling liquid through axisymmetrical phaseguides. A special type of hollow cantilever was devised to test this theory and to determine the static contact angle. In line with the prediction, the burst pressure plateaus from the critical angle β_{c2} onwards. The static contact angle was found to be in the range of 60° to 66°.

The application of axisymmetrical phaseguides to femtopipettes holds great promise as a multifunctional tool in micro-engineering, micro-chemistry, and micro-biology. The provided designs are well suited to be complemented with AFM functionality, opening the door to exciting next steps in single-cell research.

6. Experimental Section

Fabrication Methods: Fluid Interface: The assembly of fluid interfaces and support-cups was printed with a DLP printer (Micro Plus HiRes, EnvisionTEC GmbH) with a layer height of 35µm using a proprietary recipe (HTM140v2, EnvisionTEC GmbH) in combination with a transparent methacrylate/acrylate-based photoresist (3DM Tough Clear, ADMAT SASU). Prints were cleaned with IPA (99.8% Honeywell, Riedel-de-Haën) and post-cured with UV light (Photopol A5406, Dentalfarm).

Next, the apertures were created with laser abblation (WS Starter micro-machining laser system, Optec S.A.), employing a laser power of 15W at 50kHz with a writing speed of 15mm s^{-1} and 15 repetitions.

The last step before 2PP printing was to briefly sputter the fluid interfaces with a 3nm gold layer (JEOL JFC1300 sputter coating system) using a sputtering current of 10 mA during 5 s with 20 mm target-substrate distance. This step enhanced the reflectivity of the surface, which enabled automatic interface finding in the 2PP printer.

Table 2. Parameters of the two-photon-polymerization printing process.

	Dome	Cantilever	Nozzle
Laser power*	60%	50%	40%
Scanning speed [mm s^{-1}]	70	40	50
Slicing distance [µm]	0.35	0.2	Adaptive (0.05-0.3)
Hatching distance [µm]	0.25	0.2	0.15
Galvo acceleration [V/ms^{-2}]	6	6	2
Find interface at [µm]	5	–	–

* Laser power is given as the percentage of total laser power, which is 50mW for the used system.

After successfully 2PP printing and developing the femtopipette (see following section), the individual fluid interfaces could be removed from their sacrificial support in the support-cup with tweezers. The purge channel was then plugged by applying a small amount of 3DM Tough Clear resin with a dipped needle. This small resin droplet was cured for 5 min in the UV oven.

Femtopipette: The femtopipette was 3D printed on top of the fluid interface with 200 nm resolution using two-photon-polymerization (2PP) (Photonic Professional GT Laser Lithography System, Nanoscribe GmbH).

The dip-in-laser-lithography (DiLL) configuration was used in combination with a 63x magnifying objective and the IP-Dip resin (Nanoscribe GmbH). The dome was printed 5µm deeper than the fluid interface surface, to ensure good attachment and prevent leakage. Then, the cantilever was printed on the slanted channel opening of the dome. The cantilever was printed in subsequent overlapping slabs at a 45° angle to prevent sagging of the bottom layers, as well as to enable printing cantilevers with dimensions greater than the writing field. The nozzle was printed in a similar way, with parameters optimized for small cross-sectional channels (see **Table 2**). The Section S3 (Supporting Information) contains more details on the 2PP printing process.

**ADVANCED
SCIENCE NEWS**

www.advancedsciencenews.com

**small
methods**

www.small-methods.com

Upon finishing the last femtopipette print, the samples could be unloaded from the 2PP printer. The samples were developed by first submerging them in propylene-glycol-methyl-ether-acetate (PGMEA, Sigma–Aldrich) for 30 min, then in isopropanol (IPA, Sigma–Aldrich) for 5 min, and lastly in Methyl perfluoropropyl ether, 1-Methoxy-heptafluoropropane (Novec, Sigma–Aldrich) for 3 min—with gentle compressed air blow-drying in between each step. The samples were then inspected with an optical microscope to ensure all channels were cleared. An additional development cycle was needed in some batches to ensure complete channel development.

Device Characterization: After DLP printing, the fluid interfaces were inspected for obvious defects before continuing the process. Then, when the apertures were laser drilled, they were inspected and their diameter was measured with an optical microscope (Keyence Digital Microscope VHX-600). After 2PP printing, the internal channel dimensions of the 2PP printed femtopipettes could also be inspected optically, due to the transparency of the cured IP-Dip resin. However, for measuring the geometry of the smallest features such as the individual axisymmetrical phaseguides, a scanning electron microscope (SEM, Jeol JSM6010LA) was used on models with an exposed cross-section, printed with the same parameters as the complete models.

To quickly assess the functioning of each device after developing and plugging the purge channel, the individual devices were connected to a 10mL syringe with Tygon tubing and submerged in IPA. Pressure was then applied manually with the syringe to see if bubbles occurred, confirming a cleared femtopipette or indicating leakage in other areas.

Contact Angle Measurement: For the macro-scale contact angle measurement, IP-Dip was spincoated (WS-400E-6NPP-LITE, Laurell) on glass coverslips and was cured with a UV spot source (Bluepoint 4 Ecocure, Honle UV technology) for 10 min at 50mm and then developed using PGMEA and IPA according to the standard protocol (see Section S3, Supporting Information). Contact angles were measured using an optical tensiometer (Theta Lite, Biolin scientific) with DI-water (MilliQ).

The contact angle on the micro scale was assessed using the device presented in Section 4.2. The cantilever was submerged in DI-water without applied pressure. With an optical microscope, the meniscus of the fluid entering the cantilever device with varying expansion angles β was observed.

Burst Pressure Measurement: The burst pressure of the phaseguides was measured by connecting the cantilever devices through the fluid interface to a pressure sensor (Gems 3500, 0-2.5 bar ± 6.25 mbar, Gems Sensors Inc.) in series with a syringe (60mL, BD Plastipak) connected to a syringe-pump (KDS legato 111, KD Scientific Inc.). The connected device was then positioned under an optical microscope. Next, the top-surface of the device, including the cantilever, was submerged in a droplet of DI-water (ELGA Purelab Flex 3, Veolia). More details on the measurement of the burst pressure can be found in the Section S4 (Supporting Information).

Controlled Dosing: The method for observing the meniscus during the burst pressure measurement also provided a simple way to quickly assess the dosing capability of the different designed devices. For that, an empty cantilever with axisymmetrical phaseguides was submerged in DI-water and filled in steps by applying negative pressure with a handheld syringe. Next, the water inside the device was compelled back by increasing the applied pressure with the connected syringe. The pinning behavior of the liquid-air meniscus at each phaseguide step during the application of pressure was observed with the microscope.

The liquid-in-liquid dosing experiment was performed on the motorized motion stage of an AFM system (JPK BioAFM Nanowizard 4, JPK Instruments AG) in order to accurately control the position of the femtopipette. The experiment could be monitored with an embedded inverted microscope (Zeiss Axio Observer 3, Carl Zeiss Microscopy GmbH).

The device was attached to the probe holder of the AFM system whilst being connected to a pressure source (syringe, either manual or on the syringe-pump). The femtopipette was then brought within view and lowered until sufficiently close to the microscope slide, determined by the optical focus of the inverted microscope. The microscope slide could then be moved in the XY plane using the motorized stage in order to position the droplets. The diameter D_d of the pipetted droplets was then measured using the proprietary ZEN software (ZEN Blue, Carls Zeiss Microscopy GmbH).

Glycerol (Sigma–Aldrich) was added to the water to reduce evaporation of the aspirated amount when moving the femtopipette out of the droplet. The mineral oil (BioReagent light oil, Sigma–Aldrich) was first filtered using filter paper. To prevent spreading of the droplets, the glass microscope slide was first treated with siliconizing reagent (Sigmacote®, Sigma–Aldrich) in a desiccator for 1 h.

Supporting Information

Supporting Information is available from the Wiley Online Library or from the author.

Conflict of Interest

The authors declare no conflict of interest.

Data Availability Statement

The data that support the findings of this study are available from the corresponding author upon reasonable request.

[1] S. Lindström, H. Andersson-Svahn, *Lab Chip* **2010**, *10*, 3363.
[2] J. R. Heath, A. Ribas, P. S. Mischel, *Nat. Rev. Drug Discovery* **2016**, *15*, 204.
[3] P. Actis, *Small Methods* **2018**, *2*, 1700300.
[4] M. P. Stewart, R. Langer, K. F. Jensen, *Chem. Rev.* **2018**, *118*, 7409.
[5] G. Bulbul, G. Chaves, J. Olivier, R. Ozel, N. Pourmand, *Cells* **2018**, *7*, 55.
[6] P. Actis, M. M. Maalouf, H. J. Kim, A. Lohith, B. Vilozny, R. A. Seger, N. Pourmand, *ACS Nano* **2014**, *8*, 546.
[7] T. K. Chowdhury, *J. Phys. E: Sci. Instrum.* **1969**, *2*, 1087.
[8] W. Wang, Y. Sun, M. Zhang, R. Anderson, L. Langille, W. Chan, *Rev. Sci. Instrum.* **2008**, *79*, 104302.
[9] T. Hug, T. Biss, N. De Rooij, U. Staufer, in *The 13th International Conference on Solid-State Sensors, Actuators and Microsystems*, Digest of Technical Papers. TRANSDUCERS'05., Vol. 2, IEEE, Manhattan, NY USA **2005**, pp. 1191–1194.
[10] A. Meister, M. Gabi, P. Behr, P. Studer, J. Vörös, P. Niedermann, J. Bitterli, J. Polesel-Maris, M. Liley, H. Heinzelmann, T. Zambelli, *Nano Lett.* **2009**, *9*, 2501.
[11] O. Guillaume-Gentil, E. Potthoff, D. Ossola, P. Dörig, T. Zambelli, J. A. Vorholt, *Small* **2013**, *9*, 1904.

**ADVANCED
SCIENCE NEWS**

www.advancedsciencenews.com

**small
methods**

www.small-methods.com

[12] O. Guillaume-Gentil, R. V. Grindberg, R. Kooger, L. Dorwling-Carter, V. Martinez, D. Ossola, M. Pilhofer, T. Zambelli, J. A. Vorholt, *Cell* **2016**, *166*, 506.

[13] W. Chen, O. Guillaume-Gentil, P. Y. Rainer, C. G. Gäbelein, W. Saelens, V. Gardeux, A. Klaeger, R. Dainese, M. Zachara, T. Zambelli, J. A. Vorholt, B. Deplancke, *Nature* **2022**, *608*, 733.

[14] C. G. Gäbelein, Q. Feng, E. Sarajlic, T. Zambelli, O. Guillaume-Gentil, B. Kornmann, J. A. Vorholt, *PLoS Biol.* **2022**, *20*, e3001576.

[15] O. Guillaume-Gentil, C. G. Gäbelein, S. Schmieder, V. Martinez, T. Zambelli, M. Künzler, J. A. Vorholt, *Commun. Biol.* **2022**, *5*, 1.

[16] E. Potthoff, O. Guillaume-Gentil, D. Ossola, J. Polesel-Maris, S. LeibundGut-Landmann, T. Zambelli, J. A. Vorholt, *PLoS One* **2012**, *7*, 12.

[17] P. Dörig, P. Stiefel, P. Behr, E. Sarajlic, D. Bijl, M. Gabi, J. Vörös, J. A. Vorholt, T. Zambelli, *Appl. Phys. Lett.* **2010**, *97*, 1.

[18] M. K. Ghatkesar, H. H. Perez Garza, F. Heuck, U. Staufer, *Micromachines* **2014**, *5*, 954.

[19] R. C. L. N. Kramer, E. J. Verlinden, L. Angeloni, A. van den Heuvel, L. E. Fratila-Apachitei, S. M. van der Maarel, M. K. Ghatkesar, *Lab Chip* **2020**, *20*, 311.

[20] M. Knoblauch, J. M. Hibberd, J. C. Gray, A. J. Van Bel, *Nat. Biotechnol.* **1999**, *17*, 906.

[21] K. T. Rodolfa, A. Bruckbauer, D. Zhou, A. I. Schevchuk, Y. E. Korchev, D. Klenerman, *Nano Lett.* **2006**, *6*, 252.

[22] Y. T. Chow, S. Chen, R. Wang, C. Liu, C. W. Kong, R. A. Li, S. H. Cheng, D. Sun, *Sci. Rep.* **2016**, *6*, 1.

[23] P. F. J. van Altena, *Multiscale 3D printed polymer probes for single cell experiments*, Master's thesis, TU Delft, Delft, **2021**.

[24] P. Vulto, S. Podszun, P. Meyer, C. Hermann, A. Manz, G. A. Urban, *Lab Chip* **2011**, *11*, 1596.

[25] A. Glière, C. Delattre, *Sens. Actuators, A* **2006**, *130-131*, 601.

[26] P. Vulto, S. Podszun, P. Meyer, G. A. Urban, TRANSDUCERS 2009-15th International Conference on Solid-State Sensors, Actuators and Microsystems, IEEE, Denver, Colorado, USA **2009**, p. 409.

[27] I. Wenten, K. Khoiruddin, A. Hakim, N. Himma, in *Membrane Characterization*, Elsevier, Amsterdam, The Netherlands **2017**, pp. 199–218.

[28] A. D. Lantada, S. Hengsbach, K. Bade, *Bioinspir. Biomim.* **2017**, *12*, 066004.

[29] M. F. Berwind, A. Hashibon, A. Fromm, M. Gurr, F. Burmeister, C. Eberl, *Microfluid. Nanofluid.* **2017**, *21*, 1.

[30] K. Takamura, H. Fischer, N. R. Morrow, *J. Pet. Sci. Eng.* **2012**, *98-99*, 50.

[31] J. L. Pérez-Díaz, M. A. Álvarez-Valenzuela, J. C. García-Prada, *J. Colloid Interface Sci.* **2012**, *381*, 180.

[32] J.-C. Fernandez-Toledano, T. Blake, P. Lambert, J. De Coninck, *Adv. Colloid Interface Sci.* **2017**, *245*, 102.

[33] J. M. Chen, C. Y. Chen, C. H. Liu, *Jpn. J. Appl. Phys.* **2008**, *47*, 1683.